Journal Pre-proof

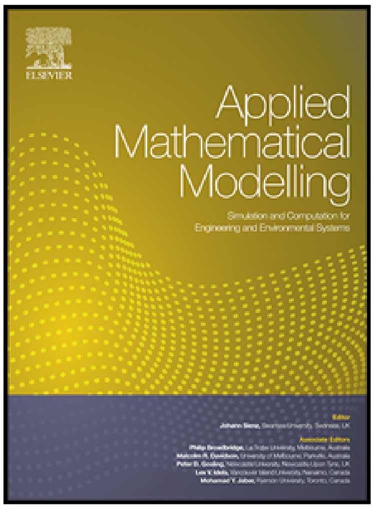

A thermodynamic constitutive model based on uncoupled physical mechanisms for polymer-based shape memory composites and its application in 4D printing

Hao Duan , Jianping Gu , Huiyu Sun , Hao Zeng , Jesus A. Rodriguez-Morales

PII: S0307-904X(25)00001-0
DOI: https://doi.org/10.1016/j.apm.2025.115926
Reference: APM 115926

To appear in: *Applied Mathematical Modelling*

Received date: 19 August 2024
Revised date: 9 December 2024
Accepted date: 2 January 2025

Please cite this article as: Hao Duan , Jianping Gu , Huiyu Sun , Hao Zeng , Jesus A. Rodriguez-Morales , A thermodynamic constitutive model based on uncoupled physical mechanisms for polymer-based shape memory composites and its application in 4D printing, *Applied Mathematical Modelling* (2025), doi: https://doi.org/10.1016/j.apm.2025.115926

Highlights

- We develop a new constitutive model for SMPs and investigate its application in 4D printing.
- Physics-based fictive temperature theory is constructed for structure relaxation.
- New stress relaxation model is proposed.
- Uncoupled physical mechanisms of structural and stress relaxation are built.
- The model can make a good prediction for three sets of experiments.

A thermodynamic constitutive model based on uncoupled physical mechanisms for polymer-based shape memory composites and its application in 4D printing

Hao Duan[1], Jianping Gu[1, 2,*], Huiyu Sun[1,*], Hao Zeng[1, 3], Jesus A. Rodriguez-Morales[1]

[1] State Key Laboratory of Mechanics and Control of Mechanical Structures, Nanjing University of Aeronautics and Astronautics, Nanjing, China

[2] Jiangsu Key Laboratory of Advanced Structural Materials and Application Technology, School of Materials Science and Engineering, Nanjing Institute of Technology, Nanjing, China

[3] School of Physical and Mathematical Sciences, Nanjing Tech University, Nanjing, China

*Corresponding authors: Jianping Gu (E-mail: gujianping@njit.edu.cn)

*Corresponding authors: Huiyu Sun (E-mail: hysun@nuaa.edu.cn)

Abstract

Four-dimensional (4D) printing is a new interdisciplinary research field that integrates sophisticated manufacturing, smart materials and mechanics. Shape memory polymer (SMP) and their composites (SMPCs) have been widely used in the field of 4D printing due to their smart and rapid response. Thus, we develop a novel thermodynamic constitutive model for SMP and SMPC, and investigate its application in 4D printing. Structure relaxation and stress relaxation are considered to follow different physical mechanisms but are related by an internal thermodynamic state variable that can represent the non-equilibrium structure. Founded on the thermodynamic variable, a physics-based fictive temperature theory is constructed for structure relaxation, and also a new stress relaxation model is proposed to characterize the time-dependent behaviors related to mechanical changes. It is shown that the influences of temperatures, strain rates, pre-strains, reinforcing fillers, and recovery conditions on stress-strain and shape memory responses are well predicted by the thermodynamic constitutive model.

Keywords: 4D printing; Shape memory polymer composites; Uncoupled physical mechanisms; Thermodynamic constitutive model

1. Introduction

4D printing integrates the knowledge of additive manufacturing, intelligent materials, and traditional mechanics, which has become a highly attractive frontier research field [1]. Note that the synergistic effect of active materials and deformation mechanisms is the critical factor in 4D printing technology. SMPs and SMPCs [2–11] are extensively utilized as active materials due to its diverse stimuli-memory effect [11, 12]. For example, comprehensive experimental research for the shape memory performance of 4D-printed SMP materials has been conducted in Refs. [8, 9]. Additionally, Rahmatabadi et al. [10, 11] suggested new 4D-printed SMPCs that can improve response speed to thermal stimuli [10] or generate responsiveness to thermo-magnetic stimuli [11]. SMPCs can also provide better mechanical properties while preserving the intrinsic characteristics of the polymer matrix [13, 14]. Theoretical modeling has significant implications for human society, such as food safety [15], disease prevention and control [16, 17], and material characterization [18–20]. Thus, we aim to utilize constitutive theory modeling to support the shape memory mechanisms, thereby providing better guidance for the application of SMPs and SMPCs in the area of 4D printing. Existing modeling methods are usually based on the thermoviscoelastic theory or the phase transition theory [21].

In literature [22], a typical phenomenological constitutive model is developed to represent the shape memory effect (SME) by hypothesizing that SMPs are composed of two switchable phases: rubbery phase (elasticity) and a glassy phase (viscosity). Subsequently, the phase transition method was further applied to represent the thermo-mechanical behaviors under large pre-deformation [23–27]. In addition, phase evolution functions had also been developed [28–30]. Nguyen et al. [31, 32] first proposed the thermoviscoelastic constitutive model coupling single-relaxation [31] and multi-relaxation [32] of structure and stress to describe the intrinsic physical mechanisms of the SME. Thereafter, the viscous flow and yield softening were incorporated into the multiple-relaxation model [32–35]. However, the number of both branches and material parameters in the multi-branch model is large, which may limit its practical application in the relevant prediction and analysis. Some studies [36–46] combine phase transition and thermoviscoelastic theories to construct constitutive models. In the work of Refs. [36–43], phase transition theory is deeply involved in the evolution of important physical quantities, viscous flow rule, and stress-strain relationships. While partial researchers only use the concept of phase transition to assist in constructing the constitutive theoretical framework [44–46].

Note that the switchable phases are phenomenological in amorphous SMPs [47]. Hence, it is plausible that thermoviscoelastic modeling approaches are better suited for the amorphous polymers. However, their thermodynamic properties in the glass transition region are complex. As a result, fictive temperature [48] is usually introduced into the thermoviscoelastic constitutive model to quantify the degree of deviation of the present thermodynamic state from equilibrium. Considerable studies have adopted this strategy [32–35, 40, 42, 43, 45, 46]. However, fictive temperature T_f is not a real thermodynamic parameter [49]. Thus, it is necessary to develop physics-based fictive temperature theory from a thermodynamic point of view.

Stress relaxation is usually assumed to show the consistent temperature dependence as structure relaxation in the constitutive modeling process [31–35], and then the coupled mechanism of the two relaxation is used to explain the shape memory effect (SME). We reconstruct the intrinsic mechanism to support the SME, and further propose a new thermodynamic constitutive model for both SMPs and SMPCs in the article. Physical stress and structure relaxation models are built with the aid of an internal thermodynamic state variable [50, 51], allowing the two relaxation to exhibit uncoupled relationship while maintaining deep cooperation. Lastly, the proposed constitutive model is applied to characterize the shape memory responses of SMPs and SMPCs under both free and constrained recovery conditions.

2. Constitutive model

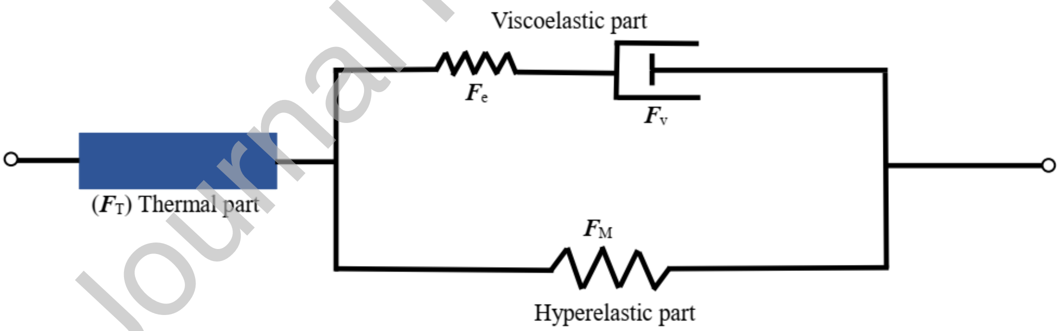

Figure 1. A brief introduction to the thermodynamic constitutive model

2.1. Kinematics

The deformation gradient tensor $\boldsymbol{F}$ and velocity gradient tensor $\boldsymbol{L}$ are defined as [41, 52]:

$$\boldsymbol{F} = \frac{\partial \boldsymbol{x}}{\partial \boldsymbol{X}}, \boldsymbol{L} = \frac{\partial(\frac{\mathrm{d}\boldsymbol{x}}{\mathrm{d}t})}{\partial \boldsymbol{X}} = \frac{\mathrm{d}\boldsymbol{F}}{\mathrm{d}t} \cdot \boldsymbol{F}^{-1} \tag{1}$$

where $\boldsymbol{X}$ represents an arbitrary material point in the reference configuration, and $\boldsymbol{x}$ is the corresponding spatial location in the current configuration at time t.

Figure 1 shows the brief introduction to the thermodynamic constitutive model. The overall deformation $\boldsymbol{F}$ is separated as follows:

$$\boldsymbol{F} = \boldsymbol{F}_{\mathrm{M}} \cdot \boldsymbol{F}_{\mathrm{T}}. \tag{2a}$$

Then, further decomposition of $\boldsymbol{F}_{\mathrm{M}}$ is conducted to acquire both the elastic and viscous deformation gradient tensors $\boldsymbol{F}_{\mathrm{e}}$ and $\boldsymbol{F}_{\mathrm{v}}$:

$$\boldsymbol{F}_{\mathrm{M}} = \boldsymbol{F}_{\mathrm{e}} \cdot \boldsymbol{F}_{\mathrm{v}}. \tag{2b}$$

The total volumetric deformation J, the volumetric deformation of the mechanical part J_{M}, and the elastic part J_{e} are respectively defined as J=det($\boldsymbol{F}$), J_{M}=det($\boldsymbol{F}_{\mathrm{M}}$) and J_{e}=det($\boldsymbol{F}_{\mathrm{e}}$). Generally, the thermal deformation $\boldsymbol{F}_{\mathrm{T}}$ of SMPs is assumed to be isotropic, as follows:

$$\boldsymbol{F}_{\mathrm{T}} = J_{\mathrm{T}}^{1/3} \boldsymbol{I} \tag{3}$$

where J_{T} is the volumetric deformation caused by temperature changes. We can decompose the tensor $\boldsymbol{L}$ into the stretching rate tensor $\boldsymbol{D}$ and spin rate tensor $\boldsymbol{W}$:

$$\boldsymbol{L} = \boldsymbol{D} + \boldsymbol{W}, \boldsymbol{D} = 0.5 \cdot (\boldsymbol{L} + \boldsymbol{L}^{\mathrm{T}}), \boldsymbol{W} = 0.5 \cdot (\boldsymbol{L} - \boldsymbol{L}^{\mathrm{T}}). \tag{4}$$

The right Cauchy-Green deformation tensors of equilibrium component $\boldsymbol{C}_{\mathrm{M}}$, elastic component $\boldsymbol{C}_{\mathrm{e}}$, and viscous component $\boldsymbol{C}_{\mathrm{v}}$ are defined as

$$\boldsymbol{C}_{\mathrm{M}} = \boldsymbol{F}_{\mathrm{M}}{}^{\mathrm{T}} \cdot \boldsymbol{F}_{\mathrm{M}}, \boldsymbol{C}_{\mathrm{e}} = \boldsymbol{F}_{\mathrm{e}}{}^{\mathrm{T}} \cdot \boldsymbol{F}_{\mathrm{e}}, \boldsymbol{C}_{\mathrm{v}} = \boldsymbol{F}_{\mathrm{v}}^{\mathrm{T}} \cdot \boldsymbol{F}_{\mathrm{v}}. \tag{5}$$

The corresponding deformation tensors, which are named left Cauchy-Green are defined as

$$\boldsymbol{B}_{\mathrm{M}} = \boldsymbol{F}_{\mathrm{M}} \cdot \boldsymbol{F}_{\mathrm{M}}{}^{\mathrm{T}}, \boldsymbol{B}_{\mathrm{e}} = \boldsymbol{F}_{\mathrm{e}} \cdot \boldsymbol{F}_{\mathrm{e}}{}^{\mathrm{T}}, \boldsymbol{B}_{\mathrm{v}} = \boldsymbol{F}_{\mathrm{v}} \cdot \boldsymbol{F}_{\mathrm{v}}^{\mathrm{T}}. \tag{6}$$

Therefore, the following relation can be obtained from the above equations, *i.e.*,

$$\boldsymbol{C}_{\mathrm{e}} = \boldsymbol{F}_{\mathrm{v}}^{-\mathrm{T}} \cdot \boldsymbol{C}_{\mathrm{M}} \cdot \boldsymbol{F}_{\mathrm{v}}^{-1}, \boldsymbol{B}_{\mathrm{e}} = \boldsymbol{F}_{\mathrm{M}} \cdot \boldsymbol{C}_{\mathrm{v}}^{-1} \cdot \boldsymbol{F}_{\mathrm{M}}^{\mathrm{T}}. \tag{7}$$

The form of Green-Lagrange strain tensor [53] is written by:

$$\boldsymbol{E} = 0.5 \cdot (\boldsymbol{F}^{\mathrm{T}} \cdot \boldsymbol{F} - \boldsymbol{I}) = 0.5 \cdot (\boldsymbol{C} - \boldsymbol{I}). \tag{8}$$

Thus, the Green-Lagrange strain tensors of equilibrium component $\boldsymbol{E}_{\mathrm{M}}$ and nonequilibrium component $\boldsymbol{E}_{\mathrm{e}}$ are defined as:

$$\boldsymbol{E}_{\mathrm{M}} = 0.5 \cdot (\boldsymbol{C}_{\mathrm{M}} - \boldsymbol{I}), \boldsymbol{E}_{\mathrm{e}} = 0.5 \cdot (\boldsymbol{C}_{\mathrm{e}} - \boldsymbol{I}). \tag{9}$$

The intrinsic mechanical property of the viscous element is strain rate dependent, necessitating the viscous velocity gradient tensor $\boldsymbol{L}_{\mathrm{v}}$. The tensor $\boldsymbol{L}_{\mathrm{v}}$ is defined in Eq. (10a) and decomposed into the viscous stretching rate tensor $\boldsymbol{D}_{\mathrm{v}}$ and viscous spin rate tensor $\boldsymbol{W}_{\mathrm{v}}$:

$$\boldsymbol{L}_{\mathrm{v}} = \frac{\mathrm{d}\boldsymbol{F}_{\mathrm{v}}}{\mathrm{d}t} \cdot \boldsymbol{F}_{\mathrm{v}}^{-1} \tag{10a}$$

and

$$\boldsymbol{L}_{\mathrm{v}} = \boldsymbol{D}_{\mathrm{v}} + \boldsymbol{W}_{\mathrm{v}}, \boldsymbol{D}_{\mathrm{v}} = 0.5 \cdot (\boldsymbol{L}_{\mathrm{v}} + \boldsymbol{L}_{\mathrm{v}}{}^{\mathrm{T}}), \boldsymbol{W}_{\mathrm{v}} = 0.5 \cdot (\boldsymbol{L}_{\mathrm{v}} - \boldsymbol{L}_{\mathrm{v}}{}^{\mathrm{T}}). \tag{10b}$$

It is noted that $\boldsymbol{W}_\text{v}$ takes as $\boldsymbol{0}$ (tensor form) without losing the generality, as discussed in Refs. [33, 41, 54], *i.e.*,

$$\boldsymbol{D}_\text{v} = \frac{\text{d}\boldsymbol{F}_\text{v}}{\text{d}t} \cdot \boldsymbol{F}_\text{v}^{-1}. \tag{11}$$

2.2. Thermodynamic consideration and constitutive equations

The thermodynamic potential function is represented by the Helmholtz free energy $\varPsi$ as follows:

$$\varPsi = u - T\eta \tag{12}$$

where the parameters η, u, and T represent the entropy, internal energy, and temperature, respectively. The internal energy of polymer is greatly affected by the mechanical work and heat flux, and it can be written by

$$\frac{\text{d}u}{\text{d}t} = \boldsymbol{P}_{\text{k}1} : \frac{\text{d}\boldsymbol{F}}{\text{d}t} - \nabla \cdot \boldsymbol{q} \tag{13}$$

where $\boldsymbol{P}_{\text{k}1}$ and $\boldsymbol{q}$ represents the first Piola–Kirchhoff stress the heat flux, respectively. The entropy inequality is given in the following form [55, 56],

$$\frac{\text{d}\eta}{\text{d}t} + \nabla \cdot \frac{\boldsymbol{q}}{T} \geq 0. \tag{14}$$

The entropy inequality can be rewritten by combining Eqs. (12)–(14) as follows,

$$-\frac{\text{d}\varPsi}{\text{d}t} + \boldsymbol{P}_{\text{k}1} : \frac{\text{d}\boldsymbol{F}}{\text{d}t} - \frac{\text{d}T}{\text{d}t}\eta - \frac{\nabla T \cdot \boldsymbol{q}}{T} \geq 0. \tag{15}$$

The equilibrium spring and the non-equilibrium spring depicted in Figure 1 store and release the free energy of SMP materials during thermo-mechanical cycling. Therefore, we can consider the thermodynamic free energy density of the material to be the sum of the equilibrium part W_M and the non-equilibrium part W_e. $\varPsi$ is taken to be a function of the tensors $\boldsymbol{C}_\text{M}$, $\boldsymbol{C}_\text{e}$, and the temperature T and can be expanded as the following form [31, 45, 46]:

$$\varPsi = W_\text{M}(\boldsymbol{C}_\text{M}, T) + W_\text{e}(\boldsymbol{C}_\text{e}, T) + W_\text{T}(T). \tag{16a}$$

W_T is related to the temperature. Then the material derivative of $\varPsi$ is expressed as

$$\frac{\text{d}\varPsi}{\text{d}t} = \frac{\partial W_\text{M}}{\partial \boldsymbol{C}_\text{M}} : \frac{\text{d}\boldsymbol{C}_\text{M}}{\text{d}t} + \frac{\partial W_\text{e}}{\partial \boldsymbol{C}_\text{e}} : \frac{\text{d}\boldsymbol{C}_\text{e}}{\text{d}t} + \frac{\partial \varPsi}{\partial T}\frac{\text{d}T}{\text{d}t}. \tag{16b}$$

The first tensor derivative formula on the right of Eq. (16b) is given by

$$\frac{\partial W_\text{M}}{\partial \boldsymbol{C}_\text{M}} : \frac{\text{d}\boldsymbol{C}_\text{M}}{\text{d}t} = 2\boldsymbol{F} \cdot \frac{\partial W_\text{M}}{\partial \boldsymbol{C}_\text{M}} : \frac{\text{d}\boldsymbol{F}}{\text{d}t}. \tag{17}$$

Besides, the second term on the right is rewritten as

$$\frac{\partial W_\text{e}}{\partial \boldsymbol{C}_\text{e}} : \frac{\text{d}\boldsymbol{C}_\text{e}}{\text{d}t} = \frac{\partial W_\text{e}}{\partial \boldsymbol{C}_\text{e}} : \frac{\partial \boldsymbol{C}_\text{e}}{\partial \boldsymbol{F}} : \frac{\text{d}\boldsymbol{F}}{\text{d}t} + \frac{\partial W_\text{e}}{\partial \boldsymbol{C}_\text{e}} : \frac{\partial \boldsymbol{C}_\text{e}}{\partial \boldsymbol{F}_\text{v}} : \frac{\text{d}\boldsymbol{F}_\text{v}}{\text{d}t} \tag{18a}$$

where the tensor derivative formulas in the right are further rewritten as

$$\frac{\partial W_{\mathrm{e}}}{\partial \boldsymbol{C}_{\mathrm{e}}}:\frac{\partial \boldsymbol{C}_{\mathrm{e}}}{\partial \boldsymbol{F}}:\frac{\mathrm{d}\boldsymbol{F}}{\mathrm{d}t}=2\boldsymbol{F}_{\mathrm{e}}\cdot\frac{\partial W_{\mathrm{e}}}{\partial \boldsymbol{C}_{\mathrm{e}}}\boldsymbol{F}_{\mathrm{v}}^{-\mathrm{T}}:\frac{\mathrm{d}\boldsymbol{F}}{\mathrm{d}t} \tag{18b}$$

and

$$\frac{\partial W_{\mathrm{e}}}{\partial \boldsymbol{C}_{\mathrm{e}}}:\frac{\partial \boldsymbol{C}_{\mathrm{e}}}{\partial \boldsymbol{F}_{\mathrm{v}}}:\frac{\mathrm{d}\boldsymbol{F}_{\mathrm{v}}}{\mathrm{d}t}=2\boldsymbol{C}_{\mathrm{e}}\cdot\frac{\partial W_{\mathrm{e}}}{\partial \boldsymbol{C}_{\mathrm{e}}}:(\frac{\mathrm{d}\boldsymbol{F}_{\mathrm{v}}}{\mathrm{d}t}\cdot\boldsymbol{F}_{\mathrm{v}}^{-1})=-2\boldsymbol{C}_{\mathrm{e}}\cdot\frac{\partial W_{\mathrm{e}}}{\partial \boldsymbol{C}_{\mathrm{e}}}:\boldsymbol{D}_{\mathrm{v}}. \tag{18c}$$

Combining Eqs. (14)–(15) yields the following form for the material derivative of $\varPsi$:

$$\frac{\mathrm{d}\varPsi}{\mathrm{d}t}=2\boldsymbol{F}\cdot\frac{\partial W_{\mathrm{M}}}{\partial \boldsymbol{C}_{\mathrm{M}}}:\frac{\mathrm{d}\boldsymbol{F}}{\mathrm{d}t}+2\boldsymbol{F}_{\mathrm{e}}\cdot\frac{\partial W_{\mathrm{e}}}{\partial \boldsymbol{C}_{\mathrm{e}}}\cdot\boldsymbol{F}_{\mathrm{v}}^{-\mathrm{T}}:\frac{\mathrm{d}\boldsymbol{F}}{\mathrm{d}t}-2\boldsymbol{C}_{\mathrm{e}}\cdot\frac{\partial W_{\mathrm{e}}}{\partial \boldsymbol{C}_{\mathrm{e}}}:\boldsymbol{D}_{\mathrm{v}}+\frac{\partial\varPsi}{\partial T}\frac{\mathrm{d}T}{\mathrm{d}t}. \tag{19}$$

The entropy inequality is further expanded as the following expression combining Eqs. (14)–(19):

$$\begin{aligned}&(\boldsymbol{P}_{\mathrm{k1}}-2\boldsymbol{F}\cdot\frac{\partial W_{\mathrm{M}}}{\partial \boldsymbol{C}_{\mathrm{M}}}-2\boldsymbol{F}_{\mathrm{e}}\cdot\frac{\partial W_{\mathrm{e}}}{\partial \boldsymbol{C}_{\mathrm{e}}}\cdot\boldsymbol{F}_{\mathrm{v}}^{-\mathrm{T}}):\frac{\mathrm{d}\boldsymbol{F}}{\mathrm{d}t}-(\eta+\frac{\partial\varPsi}{\partial T})\frac{\mathrm{d}T}{\mathrm{d}t}\\&+2\boldsymbol{C}_{\mathrm{e}}\cdot\frac{\partial W_{\mathrm{e}}}{\partial \boldsymbol{C}_{\mathrm{e}}}:\boldsymbol{D}_{\mathrm{v}}-\frac{\nabla T\cdot\boldsymbol{q}}{T}\geq 0.\end{aligned} \tag{20}$$

The value of the first two terms of Eq. (20) should be set to zero for the fulfillment of arbitrary thermodynamic processes, which leads to the following expression:

$$\boldsymbol{P}_{\mathrm{k1}}=2\boldsymbol{F}\cdot\frac{\partial W_{\mathrm{M}}}{\partial \boldsymbol{C}_{\mathrm{M}}}+2\boldsymbol{F}_{\mathrm{e}}\cdot\frac{\partial W_{\mathrm{e}}}{\partial \boldsymbol{C}_{\mathrm{e}}}\cdot\boldsymbol{F}_{\mathrm{v}}^{-\mathrm{T}}. \tag{21}$$

$\boldsymbol{P}_{\mathrm{k1}}$ is a nonsymmetrical two-point tensor [53]. Thus, the stress tensor $\boldsymbol{P}_{\mathrm{k1}}$ should be converted into the symmetric Cauchy stress tensor $\boldsymbol{\sigma}$ [31, 45, 53]. The conversion relationship [53] is as follows:

$$\boldsymbol{\sigma}=(1/\det(\boldsymbol{F}))\cdot\boldsymbol{P}_{k1}\cdot\boldsymbol{F}^{T}. \tag{22a}$$

Substituting Eq. (21) into Eq. (22a) leads to the following form:

$$\boldsymbol{\sigma}=(1/\det(\boldsymbol{F}))\cdot(2\boldsymbol{F}\cdot\frac{\partial W_{\mathrm{M}}}{\partial \boldsymbol{C}_{\mathrm{M}}}\cdot\boldsymbol{F}^{T}+2\boldsymbol{F}_{\mathrm{e}}\cdot\frac{\partial W_{\mathrm{e}}}{\partial \boldsymbol{C}_{\mathrm{e}}}\cdot\boldsymbol{F}_{\mathrm{e}}^{\mathrm{T}}). \tag{22b}$$

In consideration of the strong constraint of Eq. (21), Eq. (20) can be further simplified as

$$2\boldsymbol{C}_{\mathrm{e}}\cdot\frac{\partial W_{\mathrm{e}}}{\partial \boldsymbol{C}_{\mathrm{e}}}:\boldsymbol{D}_{\mathrm{v}}-(\nabla T\cdot\boldsymbol{q}/T)\geq 0. \tag{23}$$

The dissipative processes arising from the viscous deformation and the heat conduction are assumed to be weakly coupled, which gives

$$2\boldsymbol{C}_{\mathrm{e}}\cdot\frac{\partial W_{\mathrm{e}}}{\partial \boldsymbol{C}_{\mathrm{e}}}:\boldsymbol{D}_{\mathrm{v}}\geq 0. \tag{24}$$

To satisfy Eqs. (24), we adopt the following forms:

$$\boldsymbol{D}_{\mathrm{v}}=\frac{\boldsymbol{M}_{\mathrm{e}}}{G_{\mathrm{e}}\tau_{\mathrm{s}}} \tag{25}$$

where $\boldsymbol{M}_{\mathrm{e}}=2\boldsymbol{C}_{\mathrm{e}}\cdot(\partial W_{\mathrm{e}}/\partial\boldsymbol{C}_{\mathrm{e}})$ is the Mandel stress of the elastic part, $G_{\mathrm{e}}>0$ is the shear modulus, and $\tau_{\mathrm{s}}>0$ is the stress relaxation function.

Here, the modified Arruda-Boyce [57] model and the neo-Hookean model are chosen for W_{m} and W_{e}, respectively, which leads to

$$\begin{aligned}W_{\mathrm{M}}(\boldsymbol{C}_{\mathrm{M}},T)&=(1-V_{\mathrm{f}})\mu_{\mathrm{r}}(\lambda_{\mathrm{L}}\lambda_{\mathrm{eff}}L^{-1}(\frac{\lambda_{\mathrm{eff}}}{\lambda_{\mathrm{L}}})+\lambda_{\mathrm{L}}{}^{2}\ln(L^{-1}(\frac{\lambda_{\mathrm{eff}}}{\lambda_{\mathrm{L}}})\Big/\sinh L^{-1}(\frac{\lambda_{\mathrm{eff}}}{\lambda_{\mathrm{L}}})))\\&+V_{\mathrm{f}}((\mu_{1}/3)(\bar{I}_{\mathrm{M}}-3)+(\mu_{2}/9)(\bar{I}_{\mathrm{M}}-3)^{2})\end{aligned} \tag{26a}$$

and

$$W_{\mathrm{e}}(\boldsymbol{C}_{\mathrm{e}},T)=0.5\cdot G_{\mathrm{e}}(\bar{I}_{\mathrm{e}}-3) \tag{26b}$$

where μ_{r} is the rubbery shear modulus, λ_{L} is the number of Kuhn segments, λ_{eff} is the effective stretch, μ_1 and μ_2 are the enhancement factors, V_{f} is the volume fraction of fillers, $\bar{I}_{\mathrm{M}}=\mathrm{tr}(J_{\mathrm{M}}{}^{-2/3}\boldsymbol{B}_{\mathrm{M}})$ and $\bar{I}_{\mathrm{e}}=\mathrm{tr}(J_{\mathrm{e}}{}^{-2/3}\boldsymbol{B}_{\mathrm{e}})$. Combining Eqs. (16)–(22) and (26) yields the following form of the Cauchy stress:

$$\begin{aligned}\boldsymbol{\sigma}&=(1/J)[(1-V_{\mathrm{f}})\mu_{\mathrm{r}}\frac{\lambda_{\mathrm{L}}}{\lambda_{\mathrm{eff}}}L^{-1}(\frac{\lambda_{\mathrm{eff}}}{\lambda_{\mathrm{L}}})(\bar{\boldsymbol{B}}_{\mathrm{M}}-(\bar{I}_{\mathrm{M}}\boldsymbol{I})/3)\\&+(2/3)V_{\mathrm{f}}(\mu_{1}+(2/3)\mu_{2}(\bar{I}_{\mathrm{M}}-3))(\bar{\boldsymbol{B}}_{\mathrm{M}}-\frac{1}{3}\bar{I}_{\mathrm{M}}\boldsymbol{I})+G_{\mathrm{e}}(\bar{\boldsymbol{B}}_{\mathrm{e}}-(1/3)\bar{I}_{\mathrm{e}}\boldsymbol{I})]\end{aligned} \tag{27a}$$

where $\bar{\boldsymbol{B}}_{\mathrm{M}}=J_{\mathrm{M}}{}^{-2/3}\boldsymbol{B}_{\mathrm{M}}$ and $\bar{\boldsymbol{B}}_{\mathrm{e}}=J_{\mathrm{e}}{}^{-2/3}\boldsymbol{B}_{\mathrm{e}}$. The nonlinear evolution rule of $\boldsymbol{B}_{\mathrm{e}}$ can be characterized by the Lie time derivative [58] and the viscous stretch rate:

$$L_{\mathrm{v}}\boldsymbol{B}_{\mathrm{e}}=-2\boldsymbol{F}_{\mathrm{e}}\cdot\boldsymbol{D}_{\mathrm{v}}\cdot\boldsymbol{F}_{\mathrm{e}}{}^{\mathrm{T}}. \tag{27b}$$

2.3. Thermal deformation and Structural relaxation

Thermal deformation is significantly affected by structure relaxation across the glass transition zone. A nonequilibrium variable named fictive temperature T_{f} is usually chosen to characterize the nonlinear structure evolution of SMPs [48]. To provide a more definite physics-based description for the fictive temperature theory, a thermodynamic state variable δ is introduced to depict the nonlinear evolution of T_{f}:

$$T_{\mathrm{f}}=\frac{\rho w(\delta_{0}-\delta)}{\Delta\alpha}+T_{0} \tag{28}$$

where T_0, ρ, $\Delta\alpha$, and w are the initial temperature, material density, difference between coefficients of thermal expansion (CTEs) and coupling parameter, respectively. δ_0 is the original value of δ, and the evolution equation for the variable δ under the condition of stress-free is able to be obtained by the entropy inequality in the following form [50, 51]:

$$\frac{\mathrm{d}\delta}{\mathrm{d}t} = -(1/\tau_{\mathrm{R}})\left(\delta + (e/d)\vartheta\right) \tag{29a}$$

$$\vartheta = T - T_{\mathrm{ref}} \tag{29b}$$

$$\delta_0 = -(e/d)\left(T_0 - T_{\mathrm{ref}}\right) \tag{29c}$$

where e is a coupling parameter, d is a material parameter, T_0 is the initial temperature and ϑ is a perturbation function related to the thermodynamic equilibrium reference temperature T_{ref}. τ_{R} is the structural relaxation time, as follows:

$$\tau_{\mathrm{R}} = \tau_0 \exp\left(\frac{B}{T(\eta_{\mathrm{ref}} + \Delta\eta)}\right) \tag{30}$$

where $\Delta\eta$(t) is the perturbation function related to the thermodynamic equilibrium reference entropy η_{ref} introduced by Lion et al. [50, 51] as

$$\Delta\eta = (c_{\mathrm{p0}} / T_{\mathrm{ref}})\vartheta - e \cdot \delta \tag{31}$$

where c_{p0} is the specific heat. These structure relaxation-related parameters (w, e, d, c_{p0}) can be fitted from thermal expansion experiments as shown in Figure 3. The volume change caused by temperature is evaluated as

$$J_{\mathrm{T}} = 1 + \alpha_{\mathrm{r}}(T_{\mathrm{f}} - T_0) + \alpha_{\mathrm{g}}(T - T_{\mathrm{f}}) \tag{32}$$

where α_{r} is the coefficient of thermal expansion (CTE) in rubbery state, and α_{g} is the CTE in glassy state. α_{r} and α_{g} represent the intrinsic properties of the material, which can be directly obtained from the cited literatures.

2.4. Viscous flow and stress relaxation

The viscous flow of inelastic materials can be driven by the Mandel stress [59], as shown in Eq. (25a). It is calculated by Eq. (26b):

$$\boldsymbol{M}_{\mathrm{e}} = G_{\mathrm{e}}(\boldsymbol{C}_{\mathrm{e}} - \boldsymbol{I}). \tag{33}$$

As discussed above, the thermodynamic state variable is introduced to construct a new modified Eyring-type [31, 60, 61] stress relaxation model that can capture the influence of flow stress on relaxation, *i.e.*,

$$\tau_{\mathrm{s}} = n_{\mathrm{ref}} \exp\left(\frac{2+\delta^{-1}}{\log e} - \frac{(1+\delta^{-1})(T - T_{\mathrm{g}})}{n_{\mathrm{d}} \log e}\right)(Q/s_{\mathrm{y}})(\bar{\tau}/T)\sinh\left((Q/s_{\mathrm{y}})(\bar{\tau}/T)\right)^{-1}, \tag{34}$$

$$\bar{\tau} = \sqrt{(\boldsymbol{\sigma}_{\mathrm{e}} : \boldsymbol{\sigma}_{\mathrm{e}})/3} \tag{35}$$

and

$$\frac{\mathrm{d}s_{\mathrm{y}}}{\mathrm{d}t} = h_0(1 - (s_{\mathrm{y}}/s_{\mathrm{s}}))\frac{\sqrt{\boldsymbol{M}_{\mathrm{e}} : \boldsymbol{M}_{\mathrm{e}}}}{G_{\mathrm{e}}\tau_{\mathrm{s}}} \tag{36}$$

where Q, s_y, and $\bar{\tau}$ represent the activation parameter, yield strength, and equivalent shear stress. The parameter n_{ref} represents the viscosity, which can be determined by the equation of $n_{ref} = E_g * \tau_0$. The non-dimensional parameter n_d is related to stress relaxation, and its value is considered to be close to the viscosity parameter n_{ref}. Therefore, the viscous stretch rate tensor $\boldsymbol{D}_v$ is further represented by

$$\boldsymbol{D}_v = \frac{(\boldsymbol{C}_e - \boldsymbol{I})}{n_{ref} \exp\left(\frac{2+\delta^{-1}}{\log e} - \frac{(1+\delta^{-1})(T-T_g)}{n_d \log e}\right)(Q/s_y)(\bar{\tau}/T)\sinh\left((Q/s_y)(\bar{\tau}/T)\right)^{-1}}. \tag{37}$$

Note that Table 1 summarizes the structural equations of the thermodynamic constitutive model.

Table 1 Thermodynamic constitutive model.

Kinematics

$$\boldsymbol{F} = \boldsymbol{F}_M \cdot \boldsymbol{F}_T, \boldsymbol{F}_M = \boldsymbol{F}_e \cdot \boldsymbol{F}_v, \boldsymbol{C}_M = \boldsymbol{F}_M{}^T \cdot \boldsymbol{F}_M, \boldsymbol{B}_M = \boldsymbol{F}_M \cdot \boldsymbol{F}_M{}^T, \boldsymbol{C}_e = \boldsymbol{F}_e{}^T \cdot \boldsymbol{F}$$

$$\boldsymbol{B}_e = \boldsymbol{F}_e \cdot \boldsymbol{F}_e{}^T, \boldsymbol{E}_M = 0.5 \cdot (\boldsymbol{C}_M - \boldsymbol{I}), \boldsymbol{D}_v = (\mathrm{d}\boldsymbol{F}_v / \mathrm{d}t) \cdot \boldsymbol{F}_v{}^{-1}$$

Thermal deformation

$$J_T = 1 + \alpha_r (T_f - T_0) + \alpha_g (T - T_f), T_f = \frac{\rho w(\delta_0 - \delta)}{\Delta\alpha} + T_0$$

$$\frac{\mathrm{d}\delta}{\mathrm{d}t} = -\frac{1}{\tau_R}\left(\delta + (e/d)\vartheta\right), \tau_R = \tau_0 \exp\left(\frac{B}{T(\eta_{ref} + \Delta\eta)}\right)$$

Stress response

$$\boldsymbol{\sigma} = (1/J)[(1-V_f)\mu_r \frac{\lambda_L}{\lambda_{eff}} L^{-1}(\frac{\lambda_{eff}}{\lambda_L})(\bar{\boldsymbol{B}}_M - (\bar{I}_M \boldsymbol{I})/3)$$

$$+(2/3)V_f(\mu_1 + (2/3)\mu_2(\bar{I}_M - 3))(\bar{\boldsymbol{B}}_M - \frac{1}{3}\bar{I}_M \boldsymbol{I}) + G_e(\bar{\boldsymbol{B}}_e - (1/3)\bar{I}_e \boldsymbol{I})]$$

$$L_v \boldsymbol{B}_e = -2\boldsymbol{F}_e \cdot \boldsymbol{D}_v \cdot \boldsymbol{F}_e{}^T, \boldsymbol{D}_v = \boldsymbol{M}_e / (G_e \tau_s)$$

$$\tau_s = n_{ref} \exp\left(\frac{2+\delta^{-1}}{\log e} - \frac{(1+\delta^{-1})(T-T_g)}{n_d \log e}\right)(Q/s_y)(\bar{\tau}/T)\sinh\left((Q/s_y)(\bar{\tau}/T)\right)^{-1}$$

3. Results and discussion

Three sets of test data are applied to test the availability and precision of the constitutive model. All the calculation results are obtained by home-developed C++ code. A detailed description of the experimental condition can be found in Wang et al. [20], Westbrook et al. [33], and Yang et al. [62]. The model parameters are listed in Tables 2, 3 and 4.

Table 2 Parameters of the models for SMP [33].

Parameters	Values	Parameters	Values
T_g	40°C	ρ	1050 kg/m^3

μ_N	2.2MPa	n_{ref}	21MPa/s
λ_L	1.14	$E_1/E_2/E_3$	676/1871/5.0MPa
Q	5799K	$T_1/T_2/T_3$	22.2/31/142.5oC
α_r	2.52×10^{-4} /°C	$m_1/m_2/m_3$	19.3/58.35/177.6
α_g	1.25×10^{-4} /°C	τ_0	3×10^{-2}s
B	20000J/kg	η_{ref}	6.0J/Kg • K
C_{p0}	50J/Kg • K	n_d	15
e	1.5×10^{-9} J/Kg • K	d	1.5×10^{-17} J/Kg
w	1.1×10^{-15} m^3/ kg	v	0.49
T_{ref}	25°C	E_g	700MPa
s_0, s_s	58MPa, 35MPa	h_0	600MPa

Table 3 Parameters of the models for 4D-printed SMP [20].

Parameters	Values	Parameters	Values
T_g	59°C	ρ	1050 kg/m^3
μ_r	1.33MPa	n_{ref}	39MPa/s
λ_L	4.5	$E_1/E_2/E_3$	755/93.9/8MPa
Q/s_y	101K/MPa	$T_1/T_2/T_3$	26/39/65°C
v	0.49	$m_1/m_2/m_3$	57.26/53.9/177
α_g	1.1×10^{-4}/°C	τ_0	3.5×10^{-2}s
α_r	2.0×10^{-4}/°C	η_{ref}	9.6J/Kg • K
C_{p0}	65J/Kg • K	n_d	27.8
e	1.5×10^{-9}J/kg • K	d	4.9×10^{-17} J/kg
w	$1.1\times10^{-15}$$m^3$/ kg	V_f	0
T_{ref}	55°C	E_g	1116MPa

Table 4 Parameters of the models for SMP and their composites [62].

Parameters	Values(SMP, SMPC)	Parameters	Values(SMP, SMPC)
T_g	55°C, 50.4 °C	ρ	1050 kg/m^3
μ_r	0.25MPa	n_{ref}	47.9MPa/s
λ_L	1.303	$E_1/E_2/E_3$	3369/129/3MPa, 4709/182/10MPa
Q/s_y	1299K/MPa	$T_1/T_2/T_3$	26/45/142.5°C, 26/43.99/142.5°C
v	0.49	$m_1/m_2/m_3$	57.26/53.35/177.58,57.26/73.35/177.58
α_g	1.4×10^{-4}/°C	τ_0	3×10^{-2}s
α_r	2.62×10^{-4}/°C	η_{ref}	2.2J/Kg • K
C_{p0}	80J/Kg • K	n_d	33.5
e	4.5×10^{-9}J/kg • K	d	1.5×10^{-16} J/kg
w	$1.81\times10^{-14}$$m^3$/ kg	V_f	0, 0.04
T_{ref}	33°C	E_g	1600MPa, 2262MPa
μ_1	0,35MPa;	μ_2	0, 8.75MPa

3.1. Determination of the model parameters

The hyperelastic parameters, μ_r, μ_1, μ_2, and λ_L, are determined by fitting the stress-strain curves above T_g as shown in Figures 5, 6, and 7.

The modulus of the polymer matrix is significantly affected by the temperature in the following form:

$$E_{\mathrm{m}} = E_1 \exp[-(T / T_1)^{m_1}] + E_2 \exp[-(T / T_2)^{m_2}] + E_3 \exp[-(T / T_3)^{m_3}] \tag{38}$$

where the above equation originates from the Prony series theory. The stiffness of SMPC in the glassy state is predicted by the following mixture rule:

$$E_{\mathrm{c}} = V_{\mathrm{f}} E_{\mathrm{f}} + (1 - V_{\mathrm{f}}) E_{\mathrm{m}} \tag{39}$$

where E_{m} and E_{f} represent Young's moduli of matrix and reinforcing filler, respectively. The symbol V_{f} represents the volume fraction of reinforcing fillers. Figure 2 presents the model results calculated by Eq. (36) and the test data for the Young's moduli, respectively.

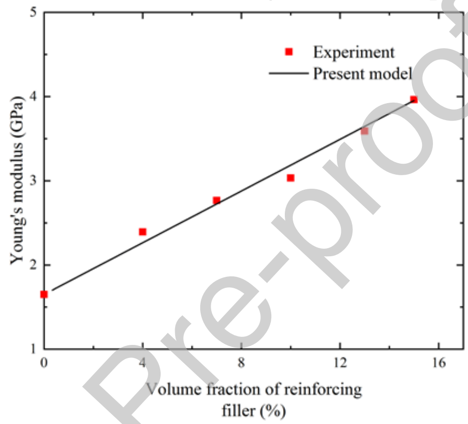

Figure 2. Relationship of Young's modulus and reinforcing filler [62].

The two sets of thermal expansion experiments are conducted by reducing the ambient temperature from 373K to 273K in 100 min and 353K to 293K in 30min, respectively. The conditions for the thermal expansion experiments are that the testing temperature decreases from (a) 100°C to 0°C [33] and (b) 80°C to 20°C [20] at the speed of 1°C /min and 2°C/min, respectively. The testing results and theoretical predictions of the thermal expansion experiments are shown in Figure 3.

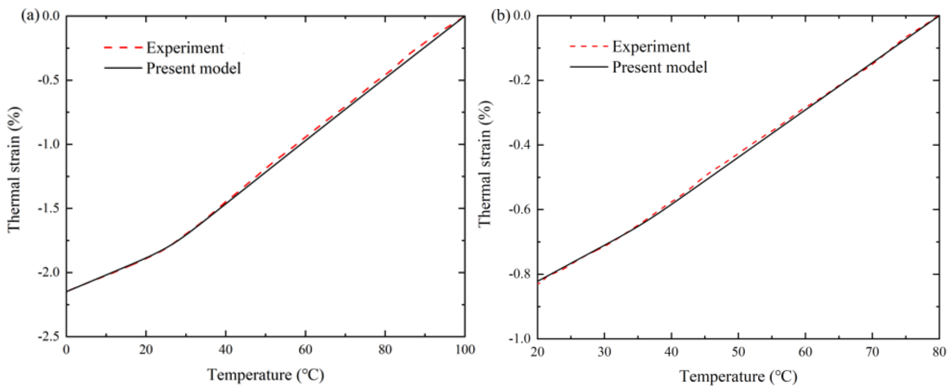

Figure 3. Both the model results and the testing data for the thermal expansion experiments of (a) the general SMP [33] and (b) the 4D-printed SMP [20].

3.2. Stress-strain response

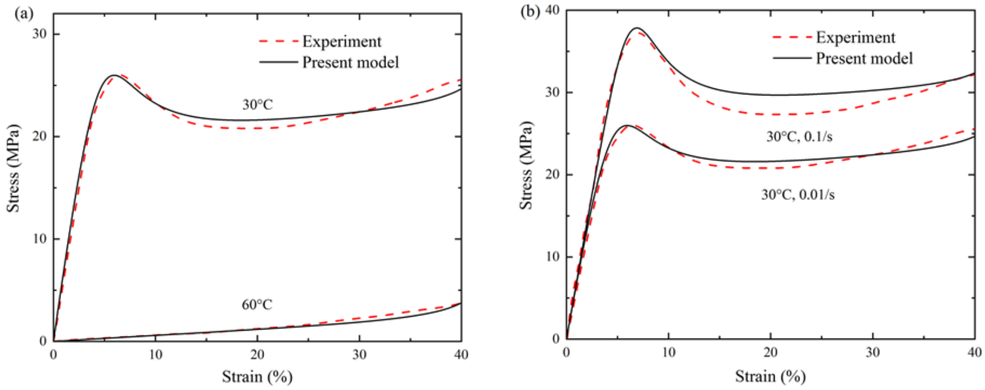

Figure 4. Uniaxial compression behaviors of general SMPs [33] at different (a) temperatures and (b) strain rates.

The stress-strain relationship affected by both the strain rate and the temperature is researched in the uniaxial compression test, as shown in Figure 4. It is obvious that the characteristic viscoplastic response transfers to the viscoelastic response as temperature increases. Moreover, the yield limit is significantly improved by increasing the strain rate, but the softening trends remain almost unchanged at different strain rates. It is clear that the stress response is well predicted by the constitutive model during the loading procedure.

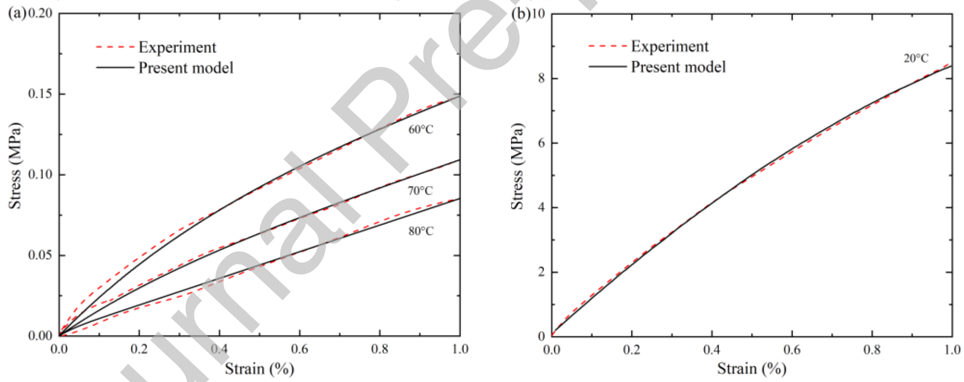

Figure 5. Stress-strain curves for 4D-printed SMPs [20] programmed at (a) rubbery temperatures and (b) glassy temperatures.

Wang et al. [20] conducted uniaxial tension experiment on 4D-printed samples at a constant force load of 6 N/min, but at different temperatures. Note that this test is limited to the linear elasticity deformation range, and thus yield softening did not occur below T_g. With appropriate model parameters, the stress responses of printed SMPs can be accurately reproduced by the theoretical analysis, which is shown in Figure 5.

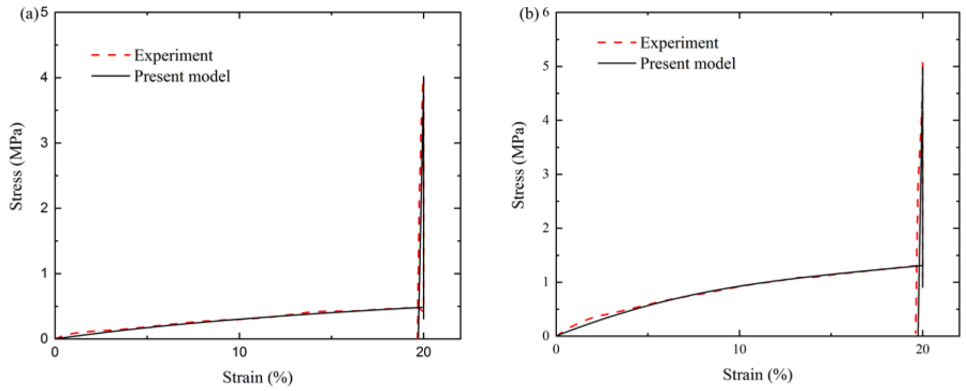

Figure 6. Relation between stress and strain of the first three steps [62] for (a) SMP and (b) SMPC in a shape memory cycle.

Figure 6 shows the stress responses in the steps of loading, cooling, and unloading for SMP and carbon powder-reinforced SMPC (volume fraction of reinforcing fillers V_f=4%). Both the SMP and SMPC specimens were uniaxially stretched to 20% at T_g+10°C at a strain rate (5×10^{-3}/s) in the study of Yang et al. [62]. Subsequently, the specimens were cooled down to 25°C (1°C /4.5s), and then the external load is unloaded. It is visible that the constitutive model can successfully describe the enhancement effect of carbon powder on the hyperelastic behavior in the tensile process. Moreover, model results and experimental data are almost completely consistent, which is different from a certain deviation for the low-temperature stress-strain behaviors in Figure 4. The main reason may be that the viscosity is extremely weak at high temperatures above T_g, *i.e.*, materials do not show significant time dependence, which leads to easier representation of their thermo-mechanical behaviors to a certain extent. In addition, the high-temperature stress-strain response in Figure 4a also supports our hypothesis.

3.3. Free recovery response

Next, the model is employed to reproduce the free recovery behaviors. According to Westbrook et al. [33], the free shape memory cycle includes five steps: (1) The sample was firstly programmed at a strain rate of -0.01/s at T_{H1} (40°C); (2) Subsequently, the programmed sample was allowed to relax for 10 min at T_{H1}; (3) The ambient temperature was cooled down to T_L (10°C) in 8 min; (4) The cooled sample was given one hour to achieve shape fixity; (5) Finally, the sample was reheated to a high temperature of T_{H2} (50°C) in 12 min and then continued to be insulated for 48 minutes to attain shape recovery. In the research of Ge et al. [20], the cycle was relatively concise. The 4D-printed sample was stretched by 6% at 80°C at a strain rate of 0.001/s, then was cooled down to 20°C in 30 min to maintain the strain, and finally was heated to 80 °C to realize the recovery. It is clear that both the general sample and 4D-printed sample can almost achieve complete shape recovery. Our constitutive model provides good theoretical predictions for free recovery of both general SMP and 4D-printed SMP, as shown in Figure 7.

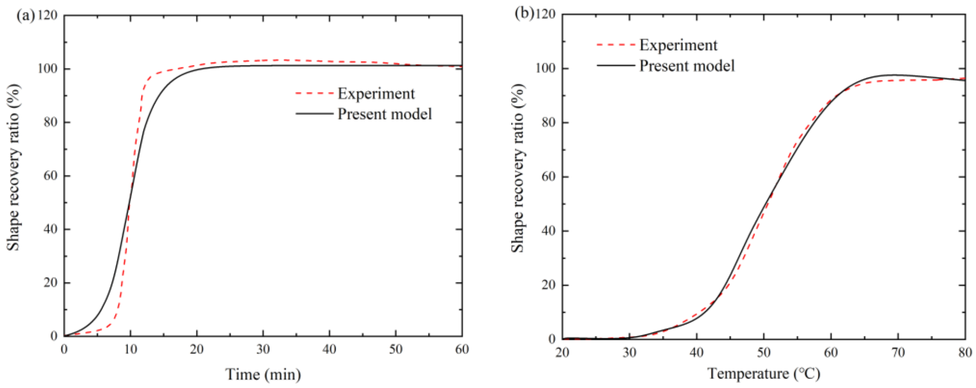

Figure 7. Model results versus experiments for the shape recovery of (a) the general SMP [33] and (b) the 4D-printed SMP [20].

Figure 8 shows the theoretical prediction for the shape recovery ratio. Following the first 3 steps in Figures 6a and 6b, both the SMP and carbon powder-reinforced SMPC (V_f=4%) specimens were reheated to nearly 80°C at a rate of 2°C/min to restore their original shape. The test data shows that the shape recovery performance can be influenced by the reinforced fillers. The main reason is that T_g is significantly affected by the fillers. The model can still well describe the shape-recovery behaviors of both SMP and SMPC. Moreover, the model results decrease after reaching a peak when the temperature is above the programming temperature, as shown in Figure 8(a). However, the drop in the final shape recovery stage of composites almost disappears, which resulted from the limit of fillers on the thermal strain. Thus, the temperature factor needs to be considered in the constitutive model in the future.

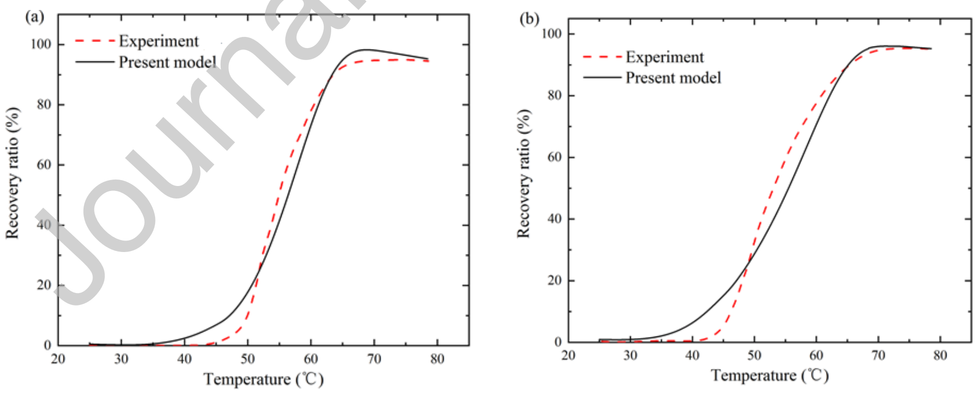

Figure 8. Model results versus experiments [62] for the shape recovery of (a) SMP and (b) SMPC.

3.4. Stress recovery response

Finally, the model is applied to simulate the constrained stress recovery response. According to Westbrook et al. [33], the previous four steps in the constrained shape memory cycle are similar to those in free recovery, except T_{H1} was set at 60°C. A significant difference between constrained and free recovery occurs in the final step, *i.e.*, the stress recovery was achieved by reheating the sample to 60°C in 20 min in a constrained state. After the first 3 steps shown in Figure 6b, the specimen with a tensile pre-strain of 20% was fixed and heated to 70°C in the work of Yang et al. [62]. Figure 9 shows the results derived from both the experimental testing and the present model for constrained recovery of SMP and SMPC.

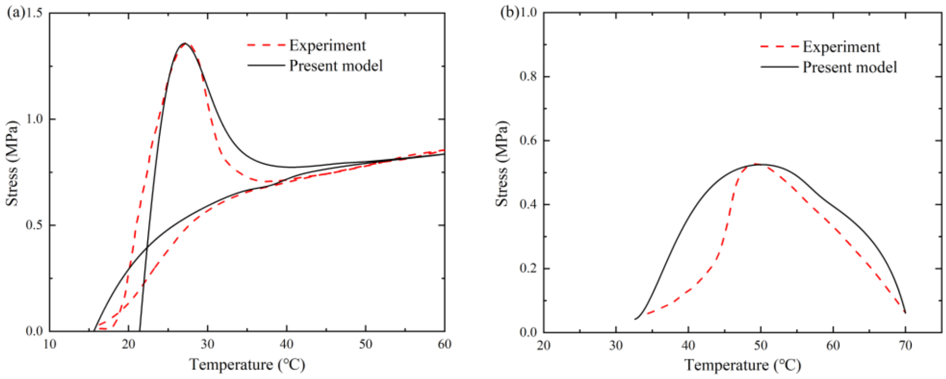

Figure 9. Model results versus experiments for the stress recovery of (a) SMP [33] and (b) SMPC [62].

As shown in Figure 9a, the stress diminishes progressively as the cooling process advances. When the temperature rises above T_g during the reheating process, the stress increases beyond its initial level, which is called stress overshoot. As the temperature continues to rise, the stress drops from its peak to the initial value (termed stress memory) of the cooling stage. The theoretical model's slower activation of viscous flow causes slight deviations in the early stages of the reheating process. However, our constitutive model can capture the stress overshoot and stress memory and provide effective calculation results that are generally consistent with experiments.

The stress recovery behavior of carbon powder-reinforced SMPC (V_f=4%) can be found in Figure 9b. The stress recovery curve shows a visible parabolic trend, *i.e.*, the value decreases to near zero at around the final reheating temperature after reaching a peak. Moreover, the stress overshoot and stress memory shown in Figure 9a did not occur here. It may be inferred that stress recovery characteristics are related to the type of programming load. Figure 9b reveals that the constitutive model simulates a faster viscous flow than the test, leading to slight errors in the glassy temperature region. However, the peak of the recovery stress overlaps between the model result and the experiment, providing a rough proof of the accuracy of our constitutive model.

4. Conclusions

To provide effective guidance for the design of 4D-printed SMP materials and describe the shape-memory properties of materials, a novel thermodynamic constitutive theory incorporating uncoupled physical mechanisms of structural and stress relaxation is developed. Specifically, we construct physical structure and stress relaxation models that can deeply collaborate but show distinct temperature dependence on the basis of the thermodynamic state variable, ultimately establishing the entire constitutive theory framework. A series of thermo-mechanical experiments are used to prove the rationality of the theoretical predictions.

The simulated results mean that the constitutive model can effectively represent the mechanical performance and shape memory performance of testing materials. Despite the lack of specific experimental data for 4D-printed SMPCs, our constitutive model has been verified using mechanical experiments and shape memory experiments from both 4D-printed SMPs and general SMPCs. Therefore, this model can also be applied to 4D-printed SMPCs by adjusting partial material parameters. Moreover, other particle-reinforced SMPCs can also be predicted by this constitutive model. It should be noted that the spectrum of relaxation times is broad for the amorphous polymers. Thus, multiple structures and stress relaxation mechanisms should be considered for the construction of the constitutive model in the future.

Acknowledgments

This work was supported by the National Natural Science Foundation of China (Grant Nos.: 12372071 and 12372070), the Special Fund of 2023 Science and Technology Plan of Jiangsu Province（the First Batch of Innovation Capacity Building Plan）, the Natural Science Foundation of Jiangsu Province of China (Grant No.: BK20220325), and the Research Fund of Nanjing Institute of Technology (CKJB202101).

Appendix A: Model implementation

The deformation gradient tensor of mechanical part $\boldsymbol{F}_{\mathrm{M}}$ is defined as:

$$\boldsymbol{F}_{\mathrm{M}} = \lambda_1 \boldsymbol{n}_1 \otimes \boldsymbol{n}_1 + \lambda_2 \boldsymbol{n}_2 \otimes \boldsymbol{n}_2 + \lambda_3 \boldsymbol{n}_3 \otimes \boldsymbol{n}_3 \tag{A.1}$$

where $\boldsymbol{n}_1$ represents the direction of mechanical deformation, and the three mutually perpendicular vectors $\boldsymbol{n}_1$, $\boldsymbol{n}_2$ and $\boldsymbol{n}_3$ are the base vectors in the coordinate system, respectively. λ_1, λ_2 and λ_3 (λ_2=λ_3) are the stretches corresponding to the three directions $\boldsymbol{n}_1$, $\boldsymbol{n}_2$ and $\boldsymbol{n}_3$, respectively. The deformation gradient tensors F_{e} and F_{v} are written as:

$$\boldsymbol{F}_{\mathrm{e}} = \lambda_{\mathrm{e}}^1 \boldsymbol{n}_1 \otimes \boldsymbol{n}_1 + \lambda_{\mathrm{e}}^2 \boldsymbol{n}_2 \otimes \boldsymbol{n}_2 + \lambda_{\mathrm{e}}^3 \boldsymbol{n}_3 \otimes \boldsymbol{n}_3 \tag{A.2}$$

and

$$\boldsymbol{F}_{\mathrm{v}} = \lambda_{\mathrm{v}}^1 \boldsymbol{n}_1 \otimes \boldsymbol{n}_1 + \lambda_{\mathrm{v}}^2 \boldsymbol{n}_2 \otimes \boldsymbol{n}_2 + \lambda_{\mathrm{v}}^3 \boldsymbol{n}_3 \otimes \boldsymbol{n}_3 . \tag{A.3}$$

According to Eq. (2b), we can derive the following multiplicative decomposition relations:

$$\begin{aligned} \lambda_1 &= \lambda_{\mathrm{e}}^1 \cdot \lambda_{\mathrm{v}}^1 \\ \lambda_2 &= \lambda_{\mathrm{e}}^2 \cdot \lambda_{\mathrm{v}}^2 \\ \lambda_3 &= \lambda_{\mathrm{e}}^3 \cdot \lambda_{\mathrm{v}}^3 . \end{aligned} \tag{A.4}$$

The isochoric left Cauchy strain tensors of the mechanical part and elastic part are written as:

$$\bar{\boldsymbol{B}}_{\mathrm{M}} = (J_{\mathrm{M}})^{-2/3} \lambda_1^{\,2} \boldsymbol{n}_1 \otimes \boldsymbol{n}_1 + (J_{\mathrm{M}})^{-2/3} \lambda_2^{\,2} \boldsymbol{n}_2 \otimes \boldsymbol{n}_2 + (J_{\mathrm{M}})^{-2/3} \lambda_3^{\,2} \boldsymbol{n}_3 \otimes \boldsymbol{n}_3 \tag{A.5}$$

and

$$\bar{\boldsymbol{B}}_{\mathrm{e}} = (J_{\mathrm{e}})^{-2/3}(\lambda_{\mathrm{e}}^{1})^{2}\boldsymbol{n}_{1}\otimes\boldsymbol{n}_{1} + (J_{\mathrm{e}})^{-2/3}(\lambda_{\mathrm{e}}^{2})^{2}\boldsymbol{n}_{2}\otimes\boldsymbol{n}_{2} + (J_{\mathrm{e}})^{-2/3}(\lambda_{\mathrm{e}}^{3})^{2}\boldsymbol{n}_{3}\otimes\boldsymbol{n}_{3} \tag{A.6}$$

where J_{M}=det[$\boldsymbol{F}_{\mathrm{M}}$]=$\lambda_1(\lambda_2)^2$, J_{e}=det[$\boldsymbol{F}_{\mathrm{e}}$]=$\lambda_{\mathrm{e}}^{1}(\lambda_{\mathrm{e}}^{2})^2$. The effective stretch λ_{chain} is specified as:

$$\lambda_{\mathrm{chain}} = (J_{\mathrm{M}})^{-1/3}\sqrt{\frac{\lambda_1^{2}+2\lambda_2^{2}}{3}}. \tag{A.7}$$

Then the Cauchy stress can be identified by

$$\boldsymbol{\sigma} = \frac{\lambda_1^{2}-\lambda_2^{2}}{(J_{\mathrm{M}})^{5/3}}(1-V_{\mathrm{f}})\mu_{\mathrm{r}}\frac{\lambda_{\mathrm{L}}}{\lambda_{\mathrm{eff}}}L^{-1}(\frac{\lambda_{\mathrm{eff}}}{\lambda_{\mathrm{L}}})\begin{bmatrix}2 & 0 & 0\\ 0 & -1 & 0\\ 0 & 0 & -1\end{bmatrix} + \frac{2}{3}V_{\mathrm{f}}(\mu_1 + \frac{2}{3}\mu_2(J_{\mathrm{M}}^{-2/3}(\lambda_1^{2}+2\lambda_2^{2})-3))\frac{\lambda_1^{2}-\lambda_2^{2}}{J_{\mathrm{M}}}\begin{bmatrix}2 & 0 & 0\\ 0 & -1 & 0\\ 0 & 0 & -1\end{bmatrix}$$
$$+\frac{(\lambda_{\mathrm{e}}^{1})^{2}-(\lambda_{\mathrm{e}}^{2})^{2}}{J_{\mathrm{M}}(J_{\mathrm{e}})^{2/3}}G_{\mathrm{e}}\begin{bmatrix}2 & 0 & 0\\ 0 & -1 & 0\\ 0 & 0 & -1\end{bmatrix}. \tag{A.8}$$

References

[1] X. Kuang, D.J. Roach, J. Wu, C.M. Hamel, Z. Ding, T. Wang, M.L. Dunn, H.J. Qi, Advances in 4D printing: materials and applications, Adv. Funct. Mater. 29(2019), 1805290. https://doi.org/10.1002/adfm.201805290.

[2] Q. Ge, H.J. Qi, M.L. Dunn, Active materials by fourdimension printing, Appl. Phys. Lett. 103(2013), 131901. https://doi.org/10.1063/1.4819837.

[3] X. Wang, Y. He, Y. Liu, J. Leng, Advances in shape memory polymers: Remote actuation, multi-stimuli control, 4D printing and prospective applications, Mat. Sci. Eng. R. 151(2022), 100702. https://doi.org/10.1016/j.mser.2022.100702.

[4] C. Yuan, F. Wang, B. Qi, Z. Ding, D. W. Rosen, Q. Ge, 3D printing of multi-material composites with tunable shape memory behavior, Mater. Design. 193(2020), 108785. https://doi.org/10.1016/j.matdes.2020.108785.

[5] X. Wan, Y. He, Y. Liu, J. Leng, 4D printing of multiple shape memory polymer and nanocomposites with biocompatible, programmable and selectively actuated properties, Addit. Manuf. 53(2022), 102689. https://doi.org/10.1016/j.addma.2022.102689.

[6] M. Y. Khalid, Z. U. Arif, R. Noroozi, A. Zolfagharian, M. Bodaghi, 4D printing of shape memory polymer composites: A review on fabrication techniques, applications, and future perspectives, J. Manuf. Process. 81(2022) 759–797. https://doi.org/10.1016/j.jmapro.2022.07.035.

[7] C. Yuan, Z. Ding, T.J. Wang, M.L. Dunn, H.J. Qi, Shape forming by thermal expansion mismatch and shape memory locking in polymer/elastomer laminates, Smart. Mater. Struct. 26(2017), 105027. https://doi.org/10.1088/1361-665X/aa8241.

[8] M. Aberouman, D. Rahmatabadi, K. Soltanmohammadi, E. Soleyman, I. Ghasemi, M. Baniassadi, K. Abrinia, M. Bodaghi, M. Baghani, Stress recovery and stress relaxation behaviors of PVC 4D printed by FDM technology for high-performance actuation applications, Sensor. Actuat. A-Phys. 361(2023), 114572. https://doi.org/10.1016/j.sna.2023.114572.

[9] D. Rahmatabadi, K. Soltanmohammadi, M. Aberoumand, E. Soleyman1, I. Ghasemi, M. Baniassadi, K. Abrinia, M. Bodaghi, M. Baghani, 4D printing of porous PLA-TPU structures: effect of applied deformation, loading mode and infill pattern on the shape memory performance, Phys. Scripta. 99(2024), 025013. https://doi.org/10.1088/1402-4896/ad1957.

[10] D. Rahmatabadi, M. Khajepour, A. Bayati, K. Mirasadi, M. A. Yousefi, A. Shegeft, I. Ghasemi, M. Baniassadi,

K. Abrinia, M. Bodaghi, M. Baghani, Advancing sustainable shape memory polymers through 4D printing of polylactic acid-polybutylene adipate terephthalate blends, Eur. Polym. J. 216(2024), 113289. https://doi.org/10.1016/j.eurpolymj.2024.113289.

[11] D. Rahmatabadi, K. Mirasadi, A. Bayati, M. Khajepour, I. Ghasemi, M. Baniassadi, K. Abrinia, M. Bodaghi, M. Baghan, 4D printing thermo-magneto-responsive PETG-Fe3O4 nanocomposites with enhanced shape memory effects, Appl. Mater. Today. 40(2024), 102361. https://doi.org/10.1016/j.apmt.2024.102361.

[12] H. Meng, G. Li, A review of stimuli-responsive shape memory polymer composites, polymer 54(2013) 2199–2221. https://doi.org/10.1016/j.polymer.2013.02.023.

[13] R. Zhang, J. Tian, Y.H. Wu, W.M. Chou, J.Y. Yang, P. Xue, An investigation on shape memory behaviors of UHMWPE-based nanocomposites reinforced by graphene nanoplatelets, Polym. Test. 99(2021), 107217. https://doi.org/10.1016/j.polymertesting.2021.107217.

[14] E.T. Thostenson, C. Li, T.W. Chou, Nanocomposites in context, Compos. Sci. Technol. 65(2005) 491–516. https://doi.org/10.1016/j.compscitech.2004.11.003.

[15] D. Munther, S.D. Ryan, C. R. Kothapalli, N. Zekaj, Spatial characterizations of bacterial dynamics for food safety: Modeling for shared water processing environments, Appl. Math. Model. 139 (2025), 115818. https://doi.org/10.1016/j.apm.2024.115818.

[16] A. Shannon1, F. Dubeau, M. Uysal, E. Özkan, A difference equation model of infectious disease, Int. J. Bioautom. 26 (2022) 339–352. https://doi.org/10.7546/ijba.2022.26.4.000899.

[17] M. Saade, S. Ghosh, M. Banerjee, V. Volpert, Dynamics of delay epidemic model with periodic transmission rate, Appl. Math. Model. 138 (2025), 115802. https://doi.org/10.1016/j.apm.2024.115802.

[18] F. Van Loock, P.D. Anderson, R. Cardinaels, A monolithic numerical model to predict the EMI shielding performance of lossy dielectric polymer nanocomposite shields in a rectangular waveguide: design of an absorption-based sawtooth-shaped layer, Appl. Math. Model. 134 (2024) 108–125. https://doi.org/10.1016/j.apm.2024.05.029.

[19] S.M. Cai, Y.M. Chen, Q.X. Liu, Development and validation of fractional constitutive models for viscoelastic-plastic creep in time-dependent materials: Rapid experimental data fitting, Appl. Math. Model. 132 (2024) 645–678. https://doi.org/10.1016/j.apm.2024.05.008.

[20] F. Wang, C. Yuan, D. Wang, D.W. Rosen, Q. Ge, A phase evolution based constitutive model for shape memory polymer and its application in 4D printing, Smart. Mater. Struct. 29(2020), 055016. https://doi.org/10.1088/1361-665X/ab7ab0.

[21] T.D. Nguyen, Modeling shape-memory behavior of polymers, Polym. Rev. 53 (2013) 130–152. https://doi.org/10.1080/15583724.2012.751922.

[22] Y. Liu, K. Gall, M.L. Dunn, A.R. Greenberg, J. Diani, Thermomechanics of shape memory polymers: Uniaxial experiments and constitutive modeling, Int. J. Plast. 22(2006) 279–313. https://doi.org/10.1016/j.ijplas.2005.03.004.

[23] H.J. Qi, T.D. Nguyen, F. Castro, C.M. Yakacki, R. Shandas, Finite deformation thermo-mechanical behavior of thermally induced shape memory polymers, J. Mech. Phys. Solids. 56(2008) 1730–1751. https://doi.org/10.1016/j.jmps.2007.12.002.

[24] S. Reese, M. Böl, D. Christ, Finite element-based multi-phase modelling of shape memory polymer stents, Comput. Method. Appl. M. 199(2010) 1276–1286. https://doi.org/10.1016/j.cma.2009.08.014.

[25] X.G. Guo, L.W. Liu, B. Zhou, Y.J. Liu, J.S. Leng, Influence of strain rates on the mechanical behaviors of shape memory polymer, Smart. Mater. Struct. 24(2015), 095009. http://dx.doi.org/10.1088/0964-1726/24/9/095009.

[26] J.P. Gu, H.Y. Sun, C.Q. Fang, A phenomenological constitutive model for shape memory polyurethanes, J.

Intel. Mat. Syst. Str. 26(2015) 517–526. https://doi.org/10.1177/1045389X14530595.

[27] H. Park, P. Harrison, Z.Y. Guo, M.G. Lee, W.R. Yu, Three-dimensional constitutive model for shape memory polymers using multiplicative decomposition of the deformation gradient and shape memory strains, Mech. Mater. 93(2016) 43–62. https://doi.org/10.1016/j.mechmat.2015.10.014.

[28] Z.D. Wang, D.F. Li, Z.Y. Xiong, R.N. Chang, Modeling thermomechanical behaviors of shape memory polymer, J. Appl. Polym. Sci. 113(2010) 651–656. https://doi.org/10.1002/app.29656.

[29] P. Gilormini, J. Diani, On modeling shape memory polymers as elastic two-phase composite materials, Cr Mecanique. 340(2012) 338–348. https://doi.org/10.1016/j.crme.2012.02.016.

[30] Z. Pan, Z. Yu, N. Zhang, Z.S. Liu, A modified phase-based constitutive model for shape memory polymers, Polym. Int. 67(2018) 1677–1683. https://doi.org/10.1002/pi.5698.

[31] T.D. Nguyen, H.J. Qi, F. Castro, K.N. Long, A thermoviscoelastic model for amorphous shape memory polymers: incorporating structural and stress relaxation, J. Mech. Phys. Solids. 56(2008) 2792–2814. https://doi.org/ 10.1016/j.jmps.2008.04.007.

[32] T.D. Nguyen, C.M. Yakacki, P.D. Brahmbhatt, M.L. Chambers, Modeling the relaxation mechanisms of amorphous shape memory polymers, Adv. Mater. 22(2010) 3411–3423. https://doi.org/10.1002/adma.201190096.

[33] K.K. Westbrook, P.H. Kao, F. Castro, Y.F. Ding, H.J. Qi, A 3D finite deformation constitutive model for amorphous shape memory polymers: a multi-branch modeling approach for nonequilibrium relaxation processes, Mech. Mater. 43(2011) 853–869. https://doi.org/10.1016/j.mechmat.2011.09.004.

[34] R. Xiao, J. Choi, N. Lakhera, C.M. Yakacki, C.P. Frick, T.D. Nguyen, Modeling the glass transition of amorphous networks for shape-memory behavior, J. Mech. Phys. Solids. 61(2013) 1612–1635. https://doi.org/10.1016/j.jmps.2013.02.005.

[35] J.P. Gu, H.Y. Sun, C.Q. Fang, A multi-branch finite deformation constitutive model for a shape memory polymer based syntactic foam, Smart. Mater. Struct. 24(2015), 025011. https://doi.org/10.1088/0964-1726/24/2/025011.

[36] M. Baghani, R. Naghdabadi, J. Arghavani, S. Sohrabpour, A thermodynamically-consistent 3 D constitutive model for shape memory polymers, Int. J. Plast. 35(2012) 13–30. https://doi.org/10.1016/j.ijplas.2012.01.007.

[37] J.M. Guo, J.B Liu, Z.Q. Wang, X.F. He, L.F. Hu, L.Y. Tong, X.J. Tang, A thermodynamics viscoelastic constitutive model for shape memory polymers, J. Alloy. Compd. 705(2017) 146–155. https://doi.org/10.1016/j.jallcom.2017.02.142.

[38] Y. Li, Z. Liu, A novel constitutive model of shape memory polymers combining phase transition and viscoelasticity, Polymer. 143(2018) 298–308. https://doi.org/10.1016/j.polymer.2018.04.026.

[39] H. Zeng, J.S. Leng, J.P. Gu, H.Y. Sun, Modeling the thermomechanical behaviors of shape memory polymers and their nanocomposites by a network transition theory, Smart. Mater. Struct. 28(2019), 065018. https://doi.org/10.1088/1361-665X/ab1156.

[40] H. Duan, J.P. Gu, H. Zeng, A.A. Khatibi, H.Y. Sun, A thermoviscoelastic finite deformation constitutive model based on dual relaxation mechanisms for amorphous shape memory polymers, Nt. J. Smart. Nano. Mat. 14(2023) 243–264. https://doi.org/10.1080/19475411.2023.2206675.

[41] J. Li, Z. Liang, K. Chen, X. Zhang, G. Kang, Q. Kan, Thermo-mechanical deformation for thermo-induced shape memory polymers at equilibrium and non-equilibrium temperatures: Experiment and simulation, Polymer. 270(2023), 125762. https://doi.org/10.1016/j.polymer.2023.125762.

[42] J. Chen, C. Du, Q. Wang, X. Peng, A 3D finite strain constitutive model for shape memory polymers combined viscoelasticity and storage strain, Mech. Mater. 197(2024), 105103. https://doi.org/10.1016/j.mechmat.2024.105103.

[43] H. Duan, J. Gu, H. Sun, H. Zeng, A unified thermodynamic modeling approach for amorphous shape memory polymers, Comp. Mater. Sci. 246(2025), 113373. https://doi.org/10.1016/j.commatsci.2024.113373.

[44] Y. Li, Y. He, Z. Liu, A viscoelastic constitutive model for shape memory polymers based on multiplicative decompositions of the deformation gradient, Int. J. Plast. 91(2017) 300–317. http://dx.doi.org/10.1016/j.ijplas.2017.04.004.

[45] X.B. Su, X.Q. Peng, A 3d finite strain viscoelastic constitutive model for thermally induced shape memory polymers based on energy decomposition, Int. J. Plast. 110(2018) 166–182. https://doi.org/10.1016/j.ijplas.2018.07.002.

[46] Y.Y. Wang, J.C. Wang, X.Q. Peng, Refinement of a 3D finite strain viscoelastic constitutive model for thermally induced shape memory polymers, Polym. Test. 96(2021), 107139. https://doi.org/10.1016/j.polymertesting.2021.107139.

[47] H. Lu, X. Wang, K. Yu, W.M. Huang, Y. Yao, A phenomenological formulation for the shape/temperature memory effect in amorphous polymers with multi-stress components, Smart. Mater. Struct. 26(2017), 095011. https://doi.org/10.1088/1361-665X/aa77b3.

[48] A.Q. Tool, Relation between inelastic deformability and thermal expansion of glass in its annealing range, J. Am. Ceram. Soc. 29 (1946) 240–253. https://doi.org/10.1111/j.1151-2916.1946.tb11592.x.

[49] L. Leuzzi, A stroll among effective temperatures in aging systems: limits and perspectives, J. Non-Cryst. Solids. 355(2009) 686–693. https://doi.org/10.1016/j.jnoncrysol.2009.01.035.

[50] A. Lion, B. Yagimli, On the frequency-dependent specific heat and TMDSC: constitutive modelling based on thermodynamics with internal state variables, Thermochim. Acta. 490(2009) 64–74. https://doi.org/10.1016/j.tca.2009.02.016.

[51] A. Lion, J. Peters, S. Kolmeder, Simulation of temperature history-dependent phenomena of glass-forming materials based on thermodynamics with internal state variables, Thermochim. Acta. 522(2011) 182–193. https://doi.org/10.1016/j.tca.2010.12.017.

[52] M. Marin, A. Öchsner, M. M. Bhatti, Some results in Moore-Gibson-Thompson thermoelasticity of dipolar bodies, ZAMM-J. Appl. Math. Mechan. 100(2020), e202000090. https://doi.org/10.1002/zamm.202000090.

[53] J. S. Bergstrom, Mechanics of solid polymers: theory and computational modeling, William Andrew, 2015.

[54] M.C. Boyce, D.M. Parks, A.S. Argon, Large inelastic deformation of glassy polymers. part I: rate dependent constitutive model, Mech. Mater. 7 (1988) 15–33. https://doi.org/10.1016/0167-6636(88)90003-8.

[55] M.E. Gurtin, E. Fried, L. Anand, The mechanics and thermodynamics of continua, Cambridge university press, 2010.

[56] X. Rui, T. D. Nguyen, An effective temperature theory for the nonequilibrium behavior of amorphous polymers, J. Mech. Phys. Solids. 82(2015) 62–81. http://dx.doi.org/10.1016/j.jmps.2015.05.021.

[57] S. Cantournet, M.C. Boyce, A.H. Tsou, Micromechanics and macromechanics of carbon nanotube-enhanced elastomers, J. Mech. Phys. Solids. 55(2007) 1321–1339. https://doi.org/10.1016/j.jmps.2006.07.010.

[58] S. Reese, S. Govindjee, A theory of finite viscoelasticity and numerical aspects, Int. J. Solids. Struct. 35(1998) 3455–82. https://doi.org/10.1016/S0020-7683(97)00217-5.

[59] R. Xiao, H.G. Sun, W. Chen, A finite deformation fractional viscoplastic model for the glass transition behavior of amorphous polymers, Int. J. Nonlin. Mech. 93(2017) 7–14. http://dx.doi.org/10.1016/j.ijnonlinmec.2017.04.019.

[60] H. Eyring, Viscosity, plasticity, and diffusion as examples of absolute reaction rates, J. Comput. Phys. 4(1936) 283–291. https://doi.org/10.1063/1.1749836.

[61] R. Xiao, T. D. Nguyen, Modeling the solvent-induced shape-memory behavior of glassy polymers, Soft. Matter. 9(2013) 9455–9464. https://doi.org/10.1039/c3sm51210j.

[62] B. Yang, Influence of moisture in polyurethane shape memory polymers and their electrically conductive composites, Thesis(2007).

Conflicts of Interest

The authors declare that they have no known competing financial interests or personal relationships that could have appeared to influence the work reported in this paper.

Hao Duan, Jianping Gu, Huiyu Sun, Hao Zeng, Jesus A. Rodriguez-Morales